Publ. Astron. Soc. Japan (2014) 00(0), 1–9
doi: 10.1093/pasj/xxx000

arXiv:1605.05408v1 [astro-ph.SR] 18 May 2016

Superoutburst of CR Bootis: Estimation of Mass Ratio of a typical AM CVn star by Stage A Superhumps

Keisuke ISOGAI,[1*] Taichi KATO,[1] Tomohito OHSHIMA,[2] Kiyoshi KASAI,[3] Arto OKSANEN,[4] Kazunari MASUMOTO,[5] Daiki FUKUSHIMA,[5] Kazuki MAEDA,[5] Miho KAWABATA,[5] Risa MATSUDA,[5] Naoto KOJIGUCHI,[5] Yuki SUGIURA,[5] Nao TAKEDA,[5] Katsura MATSUMOTO,[5] Hiroshi ITOH,[6] Elena P. PAVLENKO,[7] Kirill ANTONYUK,[7] Oksana ANTONYUK,[7] Nikolai PIT,[7] Aleksei SOSNOVSKIJ,[7] Alex BAKLANOV,[7] Julia BABINA,[7] Aleksandr SKLYANOV,[8] Seiichiro KIYOTA,[9] Franz-Josef HAMBSCH,[10,11,12] Colin LITTLEFIELD,[13] Yutaka MAEDA,[14] Lewis M. COOK,[15] Gianluca MASI,[16] Pavol A. DUBOVSKY,[17] Rudolf NOVÁK,[18] Shawn DVORAK, [19] Akira IMADA,[20] Daisaku NOGAMI[1]

[1] Department of Astronomy, Kyoto University, Kyoto 606-8502, Japan
[2] Nishi-Harima Astronomical Observatory, University of Hyogo, Japan
[3] Baselstrasse 133D, CH-4132 Muttenz, Switzerland
[4] Hankasalmi observatory, Jyvaskylan Sirius ry, Verkkoniementie 30, 40950 Muurame, Finland
[5] Osaka Kyoiku University, 4-698-1 Asahigaoka, Kashiwara, Osaka 582-8582, Japan
[6] Variable Star Observers League in Japan (VSOLJ), 1001-105 Nishiterakata, Hachioji, Tokyo 192-0153, Japan
[7] Crimean Astrophysical Observatory, p/o Nauchny, 298409, Republic of Crimea
[8] Kazan Federal University, Kremlevskaya str., 18, Kazan, 420008, Russia
[9] VSOLJ, 7-1 Kitahatsutomi, Kamagaya, Chiba 273-0126, Japan
[10] Groupe Européen d'Observations Stellaires (GEOS), 23 Parc de Levesville, 28300 Bailleau l'Evêque, France
[11] Bundesdeutsche Arbeitsgemeinschaft für Veränderliche Sterne (BAV), Munsterdamm 90, 12169 Berlin, Germany
[12] Vereniging Voor Sterrenkunde (VVS), Oude Bleken 12, 2400 Mol, Belgium
[13] Department of Physics, University of Notre Dame, 225 Nieuwland Science Hall, Notre Dame, Indiana 46556, USA
[14] Kaminishiyamamachi 12-14, Nagasaki, Nagasaki 850-0006, Japan
[15] Center for Backyard Astrophysics Concord, 1730 Helix Ct. Concord, California 94518, USA
[16] The Virtual Telescope Project, Via Madonna del Loco 47, 03023 Ceccano (FR), Italy
[17] Vihorlat Observatory, Mierova 4, 06601 Humenne, Slovakia
[18] Research Centre for Toxic Compounds in the Environment, Faculty of Science, Masaryk University, Kamenice 3, 625 00 Brno, Czech Republic
[19] Rolling Hills Observatory, 1643 Nightfall Drive, Clermont, Florida 34711, USA

© 2014. Astronomical Society of Japan.

[20] Kwasan-Hida Observatory, University of Kyoto, Japan

*E-mail: *isogai@kusastro.kyoto-u.ac.jp

Received 201 0; Accepted 201 0

Abstract

We report on two superoutbursts of the AM CVn-type object CR Boo in 2014 April–March and 2015 May–June. A precursor outburst acompanied both of these superoutbursts. During the rising branch of the main superoutburst in 2014, we detected growing superhumps (stage A superhumps) whose period was $0.017669(24)$ d. Assuming that this period reflects the dynamical precession rate at the radius of the 3:1 resonance, we could estimate the mass ratio ($q = M_2/M_1$) of 0.101(4) by using the stage A superhump period and the orbital one of 0.0170290(6) d. This mass ratio is consistent with that expected by the theoretical evolutionary model of AM CVn-type objects. The detection of precursor outbursts and stage A superhumps is the second case in AM CVn-type objects. There are two interpretations of the outbursts of AM CVn-type objects. One is a dwarf nova (DN) outbursts analogy, which is caused by thermal and tidal instabilities. Another is the VY Scl-type variation, which is caused by the variation of the mass-transfer rate of the secondary. This detection of the superhump variations strongly suggests the former interpretation.

Key words: accretion, accretion disks — stars: novae, cataclysmic variables — stars: dwarf novae — stars: individual (CR Bootis)

1 Introduction

AM CVn-type objects are a rare subclass of cataclysmic variables (CVs) which are close binary systems composed of a white dwarf (WD) primary and a mass-transferring secondary star. They are characterized by absence of hydrogen lines in spectra and their ultra-short orbital periods of $\sim$5–65 min. These features suggest that the secondary is a helium WD. AM CVn-type objects are expected as one of the most promising sources of low-frequency gravitational wave (GW) radiation, which are detectable by Evolved Laser Interferometer Space Antenna (eLISA) missions (Nelemans 2013). Moreover, some of them are believed to be the progenitor of some of the type Ia supernovae (Solheim, Yungelson 2005). It is thus important to inspect the evolutionary model of AM CVn-type objects. (for reviews, see Nelemans 2005; Solheim 2010).

Three evolutionary channels (WD, He-star, and hydrogen-star channels) have been proposed to form AM CVn-type objects. The former two channels experience two common envelope (CE) events. The channels can be distinguished whether the remnant core of the donor is a degenerate WD or non-degenerate He-star. GW radiation makes the remnant cores of main-sequence (MS) stars close, and the semi-detached or detached binaries are formed. The third channel experiences one CE event and evolves in the same way as hydrogen-rich CVs. However, the binaries enable more compact orbits because of the hydrogen deficiency of the donor. The population synthesis, which depends on the birthrate in these three channels, has been discussed, but is still poorly understood. In order to investigate the population, the detailed observations are essential. By measuring the donor mass and the orbital period, we will be able to clarify whether the donor is a semi-degenerate or fully-degenerate by the theoretical equations listed below. Moreover, in each channel, the binary system once or twice experiences common envelope (CE) phases. Therefore the study of AM CVn-type objects may help elucidate yet poorly understood CE phenomena. For more details, see Deloye et al. (2007) and Solheim (2010).

Faulkner et al. (1972), Zapolsky, Salpeter (1969) and Savonije et al. (1986) derived the following equations with requirements for the Roche-lobe overflow and He-star secondary, respectively:

$$P_{\rm orb}({\rm h}) = 8.75(M_2/R_2^3)^{-1/2}, \quad (1)$$

$$R_2 = 0.0155 M_2^{-0.212} \quad \text{for the fully-degenerate secondary}, \quad (2)$$

$$R_2 = 0.029 M_2^{-0.19} \quad \text{for the semi-degenerate secondary}, \quad (3)$$

where $P_{\rm orb}$ is the orbital period, M_2 is the secondary mass and R_2 is the secondary radius in solar units, respectively. Equations (1), (2), (3) yield

$$M_2 = 0.0069 P_{\rm orb}^{-1.22} \quad \text{for the fully-degenerate secondary}, \quad (4)$$

$$M_2 = 0.018 P_{\rm orb}^{-1.27} \quad \text{for the semi-degenerate secondary}, \quad (5)$$

Based on equations (4), (5), we can draw the theoretical evolutionary tracks which represent the mass-radius relations of the

binary systems with fully and semi-degenerate secondaries. If we obtain the mass ratios of AM CVn-type objects, we can test the suitability of the evolutionary model.

Outburst phenomena in AM CVn-type objects are widely known. There is a theoretical model of outbursts in AM CVn-type objects (Tsugawa, Osaki 1997). Most of the outbursting AM CVn-type objects, whose orbital periods are $\sim$1300–2500 s, show superoutbursts and superhumps, because they have sufficiently low mass ratios and the outer edges of the disks can reach the 3:1 resonance radius ($r_{3:1}$) which causes the tidal instability (Whitehurst 1988; Osaki 1989; Lubow 1991a; Lubow 1991b; Hirose, Osaki 1990). In hydrogen-rich CVs, three stages of superhumps were discovered by Kato et al. (2009). Kato, Osaki (2013) partially succeeded in interpreting these stages of superhumps. The stage A is the growing stage of superhumps and its period is thought to reflect the dynamical precession rate at $r_{3:1}$. The pressure effect makes the superhump period suddenly shorter at the start of the stage B. The superhump period then become larger gradually. The stage C shows a constant shorter period than in the stage B, but the origin of the stage C is still unclear. On the basis of this interpretation, we can estimate the mass ratio by measurements of the stage A superhump period and the orbital one. In this paper, we applied this method to CR Boo.

2 CR Bootis

CR Boo is one of best-known AM CVn-type objects, which shows SU UMa-type outburst phenomena (Kato et al. 1999). No one, however, has ever performed time-resolved photometric observations through the superoutburst in detail. This object, called PG 1346+082, was discovered by the Palomar Green survey (Green et al. 1986). Wood et al. (1987) reported on the photometric and spectroscopic variations, and it was confirmed that this object is an interacting double white dwarf binary. The orbital period is 0.0170290(6) d (Provencal et al. 1997). Although the period variation of superhump which is similar to hydrogen-rich CVs was reported in (Kato et al. 2013), we could see the growing stage of superhumps for the first time in our present observations.

CR Boo has two distinct states: (1) fainter quiescence with regular superoutbursts state, which corresponds to the "ER UMa-like" state, and (2) brighter quiescence with frequent outbursts state (Honeycutt et al. 2013; Kato et al. 2013). During our observations, CR Boo was in the former state. ER UMa-type is a subclass of SU UMa-type CVs and is characterized by an extreme high outburst frequency and short supercycles ($\sim$19–48 d) (Kato, Kunjaya 1995), which is considered to be caused by high mass-transfer rates from the donor star (Osaki 1995). In this state, CR Boo shows a ~ 46 d supercycle (Kato et al. 1999). We can predict the date of next superoutburst by using this supercycle. We performed two observation campaigns.

3 Observation and Analysis

Our time-resolved photometric campaigns were carried out in 2014 April–May and 2015 May–June by the Variable Star Network (VSNET) collaborations (Kato et al. 2004b). The data were acquired with 20–40cm class telescopes. The logs of photometric observations are summarized in table 1 and 2 (all tables are reported only in the electronic edition). The data were observed by V-band and unfiltered CCD photometry. In the normal outbursting CVs, the magnitude of unfiltered CCD photometry is close to V-band magnitude, and we treated them in the same one. The time of the observations were corrected to barycentric Julian date (BJD). We corrected the zero-point of each observer's data by adding a constant for each observer.

We used the phase dispersion minimization (PDM) method (Stellingwerf 1978) for analyzing the periodic variations. The 1σ errors by this method were determined by the methods described in Fernie (1989) and Kato et al. (2010). Before performing period analyses, we subtracted the global trend of the light curve by subtracting smoothed light curve obtained by locally-weighted polynomial regression (LOWESS, Cleveland 1979). We used O-C diagrams which are sensitive to subtle variations of the superhump period (see Sterken 2005). We can identify stage transitions of superhumps by detecting kinks in the $O-C$ diagrams. The times of superhump maxima, which are used to draw the $O-C$ diagram, were determined by the same method as described in Kato et al. (2009).

4 Result

4.1 Overall Light Curve

The upper panel of figure 1 shows the overall light curve of CR Boo in 2014 April–May. As shown in this figure, the superoutburst lasted for 17 days. The magnitude in quiescence was $V \sim 17.2$ and the brightness rapidly increased to $V \sim 14$ on BJD 2456757. We can see a precursor outburst as a form of a "kink" in the light curve during BJD 2456757–2456758 (see the inset in the upper panel of figure 1). Following the precursor outburst, the main superoutburst began. During the plateau phase, unlike typical superoutbursts in hydrogen-rich CVs, we can see the rapid fading and brightening, which we call a "dip", with small amplitudes of $\sim$0.5–1.0 mag. The lower panel of figure 1 shows the overall light curves of CR Boo in 2015 May–June. The profile of the outburst was similar to the one in 2014, including a precursor outburst BJD 2457172-2457172.8 (see the inset in the lower panel of figure 1).

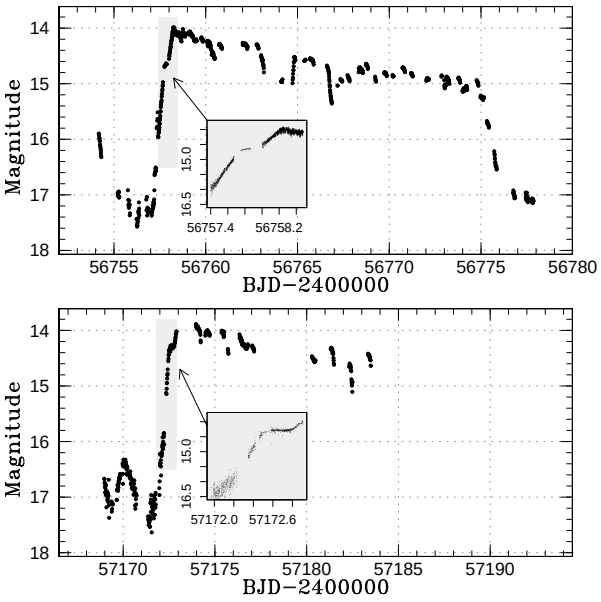

Fig. 1. Overall light curves of CR Boo in 2014 April–May (Upper panel) and in 2015 May–June (Lower panel). The observations were binned to 0.01 d. Insets: the enlarged light curves, correspond to the shaded areas, around the precursor outbursts indicated by the arrows.

4.2 Superhumps

Figure 2 shows the overall $O-C$ diagram (upper panel), and the light curve (lower panel) in the 2014 outburst. A period of 0.0172414 d, which is the stage B superhump period in 2014 we derived (see below), was used for calculating the O-C values. The times of superhump maxima are listed in table 3. As mentioned in section 1, the superhumps can be classified into three stages by the features of the variations of the periods and amplitudes. The transition of the tendency of the $O-C$ diagram around $E\sim 10$ and 700 indicates the transition of the stage A–B and B–C, respectively. Figure 3 is the enlarged figure 2 around the stage A–B transition, and shows $O-C$ diagram (upper panel), the amplitude of superhumps (middle panel), and the light curve (lower panel). We can see that the superhumps started to develop during the rapidly rising phase (around BJD 2456758) following the precursor (lower panel). As can be seen in this $O-C$ diagram, a kink can be seen at $E\sim$10, corresponding to the maximum amplitude of the superhumps and the peak of the superoutburst. These features suggest that the maxima for $E\sim$0–10 can be regarded as the stage A of superhumps. During $E=$11–26, the tendency of the $O-C$ diagram is unstable. A transition between stage A and B thus occurred in this phase. The superhump period gradually increased through the stage B ($E=$27–686) and the superhump amplitude was continuously decreased. As shown in upper panels of figure 4, the estimated mean period of the stage A in BJD 2456758.0–2456758.195, the stage B in BJD 5456758.46–2456770.0 and the stage C in BJD 2456770.7–2456779.5 are 0.017669(24), 0.017241(18) and 0.017218(5) d, respectively. The lower panels in figure 4 are the phase-averaged profiles of the stage A and the stage B. The profiles have a double-wave shape in the stage A and single-wave shape in the stage B, which match as the well-known profiles of superhumps (e.g. Kato et al. 2015).

Figure 5 shows the $O-C$ diagram of the 2015 outburst. The times of superhump or orbital hump maxima are listed in table 4. Unfortunately, the sparse data prevented us from detailed analyses of the stage A. The stage B superhumps ($E>290$) with a period of 0.017237(48) d are, however, consistent with those in the 2014 outburst. The humps during $E=$ 0–185 with a period of 0.017031(6) d appears to be the orbital ones, since their period is stably 0.017031(6) in good accordance with the previously measured one (Provencal et al. 1997). During the precursor outburst, the $O-C$ diagrams showed increasing tendency ($E=$ 214–223). Therefore we analyzed the period in BJD 2457172.55–2457173.00 where stage A superhumps were expected. We estimated the period of 0.017591(20) d with the PDM method which is in agreement with one in the 2014 within errors. Thus this phase appears to be identified as the stage A. This period, however, is not very reliable since the observation contained only three maxima and some contamination of the orbital variation may have been present. Thus, we used the period of the stage A in 2015 for just a reference.

5 Discussion

5.1 Evolution of Superhumps During the Superoutburst

In the 2014 outburst, we succeeded in detecting the evolution of superhumps. This is the first observation of the stage A superhumps in this object and the second observation in all AM CVn-type objects (Kato et al. 2014b). This fact suggests that we can apply the new method of mass-ratio estimation, which uses the stage A superhump period and the orbital period, not only for hydrogen-rich CVs but also for AM CVn-type objects. However, the stage A in the 2014 outburst was observed for a cycle count of only 10 and the duration which corresponds to the phase from the precursor to the maximum of the superoutburst is ~ 0.5 d. Thus the detection of stage A in this object is difficult. After stage A, the $O-C$ diagram for the 2014 outburst shows an unstable period during $E=$ 10–26. We therefore considered that the stage A–B transitions of superhumps occurred here.

The lower panel of figure 4 shows the profile of superhumps in the stages A and B. The transition from double-wave modulations to single-wave ones between the stage A and B is often seen in hydrogen-rich CVs (Kato et al. 2015). The period derivative $P_{\rm dot}=\dot{P}/P$ of the stage B was $1.01(2)\times 10^{-5}$ in

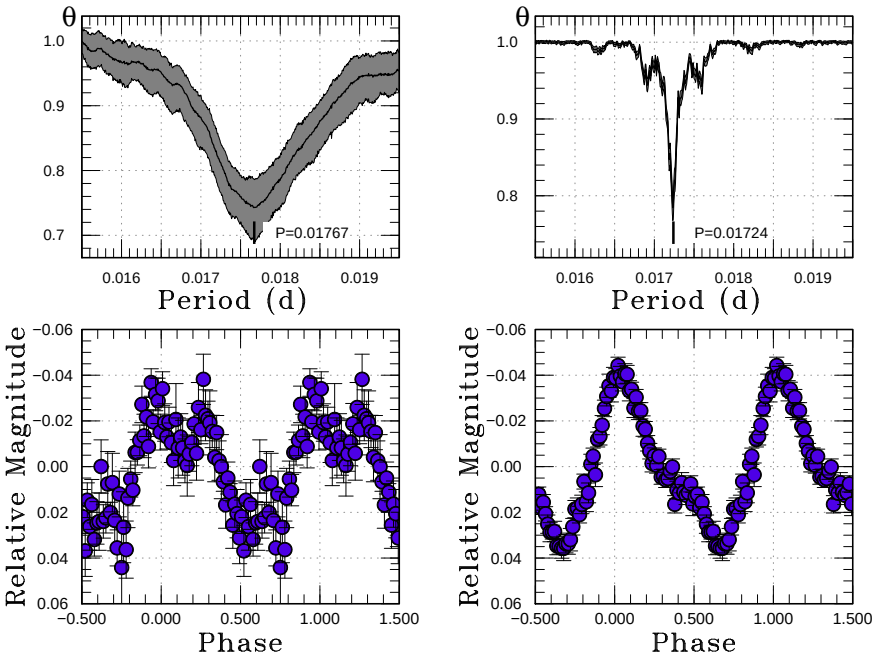

Fig. 4. Results of the period analyses of superhumps of the 2014 outburst in BJD 2456758.0–5456758.195 (Left) and in BJD 2456758.46–2456770 (Right) . (Upper): θ diagram of our PDM analysis of superhumps. The area of gray scale means 1σ errors. (Lower): Phase-averaged profiles of superhumps. The left and right panels correspond to the period analyses of the stage A and the stage B superhumps, respectively.

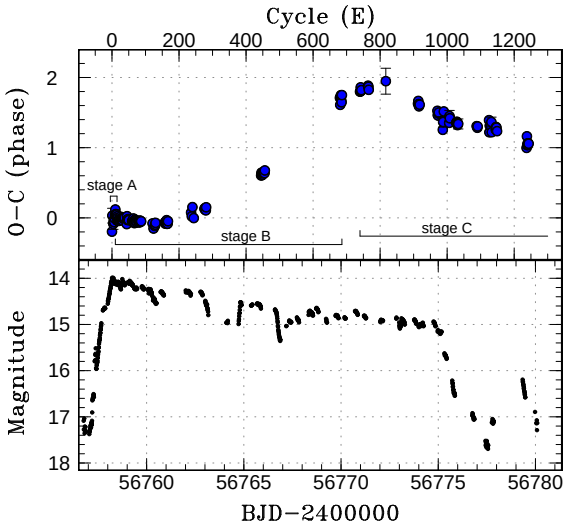

Fig. 2. (Upper) $O-C$ diagram of CR Boo during the 2014 April superoutburst. An ephemeris of Max(BJD) $= 2456758.0111 + 0.0172414E$ was used to draw this figure. The vertical axis indicates a phase (1 phase = 0.0172414 d). The intervals stage A–C represents superhump stages. (Lower) Light curve. The observations were binned to 0.01 d. The horizontal axis in units of BJD and cycle number is common to these three panels. The light curve shows two dips around BJD 2456765 and 2456767. Judging from the O-C diagram, the stage B superhumps continued through the dips. However, the presence of dips suggests that the state may have been different from stage B superhumps in hydrogen-rich CVs.

2014 and $1.76(37) \times 10^{-5}$ in 2015. Although the stage B in 2014 lasted at least for 660 cycles which is extremely long, the duration of the stage B in 2012 March was about 300 cycles (Kato et al. 2013). The presence of dips suggests that the state may have been different from stage B superhumps in hydrogen-rich CVs. Thus we assumed that the stage B in 2014 is $E =$ 27–281. The re-estimated $P_{\rm dot}(2014)$ was $1.76(12) \times 10^{-5}$ and consistent with $P_{\rm dot}(2012) = 2.0(0.2) \times 10^{-5}$ (Kato et al. 2013) and $P_{\rm dot}(2015)$. This result indicates two possibilities. The first possibility is that the stage B is not $E =$ 27–686 but 27–281. The second possibility is that $P_{\rm dot}$ depends on the stage B duration. Because $P_{\rm dot}$ is estimated on the assumption that the variation of stage B is expressed by a quadratic curve, we cannot use a parabolic curve for the fitting, if the assumption is wrong.

5.2 Outburst Behavior of CR Boo

Warner (1995) interpreted and Warner (2015) examined the typical outbursting AM CVn-type objects, whose orbital periods are 1300–2500 s, as VY Scl-type, which is characterized by the unstable mass-transfer rate. Moreover, Warner (2015) stated that "the variety of supercycle and the light curves do not convincingly support the interpretation as DN outbursts". However, the above superhump behavior clearly demonstrates that these superoutbursts are DN outbursts analogues, and the variations of the superhump period cannot be explained by the luminosity variation of VY Scl-type.

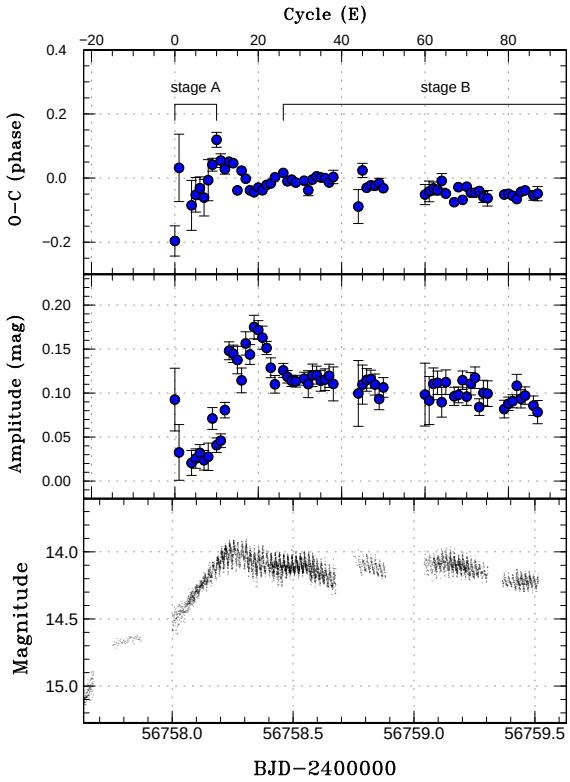

Fig. 3. Enlarged figure 2 around the stage A-B transition. (Upper) $O-C$ diagram of CR Boo during the 2014 April superoutburst. An ephemeris of Max(BJD) $= 2456758.0111 + 0.0172414E$ was used to draw this figure. The vertical axis indicates a phase (1 phase = 0.0172414 d). The intervals stage A–B represents superhump stages. (Middle) Amplitudes of superhumps. (Lower) Light curve. The horizontal axis in units of BJD and cycle number is common to these three panels.

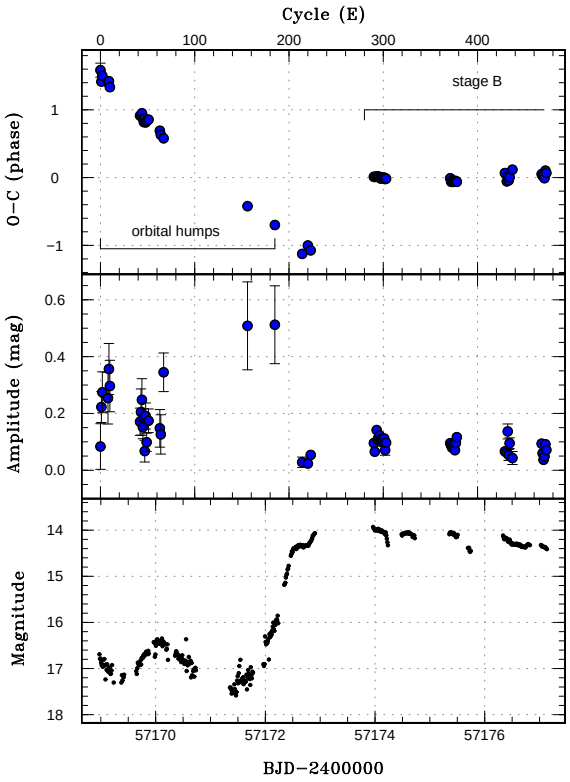

Fig. 5. (Upper) $O-C$ diagram of CR Boo during the 2015 May superoutburst. An ephemeris of Max(BJD) $= 2457168.99251 + 0.0172414E$ was used to draw this figure. The vertical axis indicates a phase (1 phase $= 0.0172414$ d). The $O-C$ diagram in $E > 290$ is similar to stage B in the 2014 outburst. The humps during $E = 0$–185 appears to be the orbital ones because of its value. Although we cannot see clear stage A superhumps. (Middle) Amplitudes of superhumps. (Lower) Light curve. The observations were binned to 0.01 d. The horizontal axis in units of BJD and cycle number is common to these three panels.

During the plateau phase, we can see two dips with amplitudes of ~ 1 mag around BJD 2456765 and 2456767 (figure 1). Such an oscillation phase of this object, which is characteristic of AM CVn-type objects (cf. Ramsay et al. 2011; Levitan et al. 2011; Levitan et al. 2015), was also observed in March 2012 (Kato et al. 2014a). The dips in AM CVn-type DNe are different from those in hydrogen-rich CVs (such as in WZ Sge-type DNe) in that they occur already early during the superoutburst plateau (cf. Kato et al. 2004a; Nogami et al. 2004). In WZ Sge-type DNe, dips or oscillations occur after the long superoutburst (Kato 2015). In helium accretion disks, it may be difficult to maintain the hot state during superoutburst.

5.3 Orbital Period of CR Boo

The well-known orbital period of CR Boo is 0.0170290(6) d (Provencal et al. 1997). This period was estimated by using the humps in quiescence. Humps in quiescence are basically caused by the hot spot in binary systems. The periods of such humps are thus regarded as the same as the orbital period. However, in binaries with an extreme high outburst frequency such as ER UMa-type objects, the binary may always have an eccentric disk and may show "permanent superhumps" (Patterson 1999). Since the CR Boo is an ER UMa-like object, the humps in quiescence may be not orbital ones. Note that the period of humps in quiescence in 2015 is consistent with the previously measured one. The orbital period by time-resolved spectroscopy is needed to be confirmed.

5.4 Estimation of the Mass Ratio from Stage A Superhumps

According to the previous work, the mass ratio of CR Boo was estimated to be 0.085 ± 0.045 (Roelofs et al. 2007).

This value is given by the empirical formula with the maximum error of 50%. By using the new method derived by Kato, Osaki (2013), we could estimate a mass ratio more accurately.

As mentioned in section 1, the period of the stage A superhumps appears to reflect the dynamical precession rate of the disk at $r_{3:1}$. Thus, the mass ratios can be measured by using the theoretical equation of the dynamical precession rate which was derived by (Hirose, Osaki 1990). This value is deflected only by the errors of $P_{\rm orb}$ and $P_{\rm SH}$ of stage A, so it has small error (for more detail, see Kato, Osaki 2013).

The fractional superhump excess ($\varepsilon^* \equiv 1 - P_{\rm orb}/P_{\rm SH}$) was 0.0362(13) in 2014 and 0.0319(11) in 2015, and we obtained mass ratios of 0.101(4) and 0.087(3), respectively. The former value 0.101(4) was adopted as the final mass ratio because of the better $O-C$ diagram as described in section 4.2.

5.5 Mass-ratio and Implications on the Evolutionary Status

Based on equations (4) and (5), we can draw the theoretical evolutionary tracks, assuming that the secondary star is semi-degenerate or fully-degenerate (Tsugawa, Osaki 1997). If we know a sufficient number of binary mass ratios, we can compare the observation with the evolutionary population synthesis of AM CVn-type objects.

We plotted the evolutionary tracks with objects whose orbital period and mass ratio are known in figure 6. The green dashed curves indicate semi-degenerate secondaries, and the red solid curves indicate fully-degenerate secondaries, respectively. From top to bottom, three lines represent the q-$P_{\rm orb}$ relation, assuming $M_1 = 0.60$, 0.75, and 1.00 $M_\odot$, respectively. Basically, assuming that the same orbital period and primary mass, the semi-degenerate secondary has a higher mass-transfer rate than the fully-degenerate one. Because the mass of the semi-degenerate secondary is needed to be heavier due to the lower density, such a binary emits stronger GW (see figures 4,5 in Nelemans et al. 2001). Figure 6 shows the secondary of CR Boo was semi-degenerate or almost non-degenerate. We could confirm that the estimated mass ratio falls within the expected range. There remain, however, possibilities that the location in the non-degenerate range may be incorrect: (1) The primary mass is smaller than the typical DNe. (2) The stage A superhump period was overestimated due to lacking data. (3) The known orbital period is incorrect (see section 5.3).

All outbursting objects (CR Boo, V406 Hya, SDSS J092620.42+034542.3, SDSS J124058.03015919, and SDSS J090221.35+381941.9) are in the semi-degenerate range (see figure 6: note that the methods of estimating q are not homogeneous). The high occurrence of objects in the semi-degenerate region may have been a result of a selection bias, since such objects are expected to have higher mass-transfer rates and they are more likely detected due to the high occurrence of outbursts.

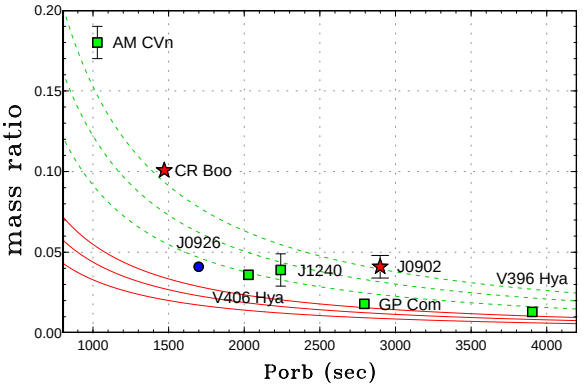

Fig. 6. Relation between q and $P_{\rm orb}$ with various primary masses. The green dashed curve indicates semi-degenerate secondaries, and the red solid curve indicates fully-degenerate secondaries. From top to bottom, three lines represent the q-$P_{\rm orb}$ relation, assuming $M_1 = 0.60$, 0.75, and 1.00 $M_\odot$, respectively. The filled stars represent the measurements from stage A superhump (J0902 (SDSS J090221.35+381941.9): Kato et al. 2014b). The filled squares represent the measurements from Doppler tomography (Marsh, Horne 1988) (AM CVn: Roelofs et al. 2006b, V406 Hya: Roelofs et al. 2006a, J1240 (SDSS J124058.03015919): Roelofs et al. 2005, GP Com: Marsh 1999, V396 Hya Solheim 2010). The filled circle represents the measurement from eclipse observations (Copperwheat et al. 2011) (J0926 (SDSS J092620.42+034542.3): Copperwheat et al. 2011).

5.6 Pressure Effect in Helium Disks

Kato et al. (2014b) suggested that we can estimate the contribution of the pressure effect by the difference between ε^* of stage A and B. The aspidal precession frequency $\nu_{\rm pr}$ is represented by the following equation (Lubow 1992): $\nu_{\rm pr} = \nu_{\rm dyn} + \nu_{\rm pressure} + \nu_{\rm stress}$, where $\nu_{\rm dyn}$, $\nu_{\rm pressure}$, and $\nu_{\rm stress}$ are disk precession frequencies due to the dynamical force of the secondary, the pressure effect, and the minor wave-wave interaction, respectively. According to Kato, Osaki (2013), stage A depends only on the first term and stage B depends on the first term and second term if we can ignore $\nu_{\rm stress}$. Therefore ε^*(stage A)$-\varepsilon^*$(stage B) corresponds to $\nu_{\rm pressure}/\nu_{\rm orb}$.

ε^*(stage A)$-\varepsilon^*$(stage B) of CR Boo are 0.025(2) in 2014 and 0.020(4) in 2015. These values are larger than those of hydrogen-rich CVs (0.010–0.015 Kato et al. (2009)) and are consistent with the suggestion by Pearson (2007) that the pressure effect in helium-rich disks appears to be higher than in hydrogen-rich disks because of the higher ionization temperature.

6 Summary

We report on photometric observations of two superoutbursts of CR Boo in 2014 April–May and 2015 May–June. we detected growing (stage A) superhumps and a precursor outburst for the second time in AM CVn-type objects, and for the first time in typical outbursting AM CVn-type objects, whose orbital

periods are 1300–2500 s. Although the outburst phenomena in AM CVn-type objects are widely known, the observations have been insufficient yet. Our observations therefore support that we can discuss AM CVn-type objects in analogy to hydrogen-rich CVs. However, during the plateau phase, we also detected characteristic oscillations of AM CVn-type objects, called dips. WZ Sge-type DNe, hydrogen-rich CVs, also show similar oscillations, nevertheless the dips or oscillations occur after a long superoutburst, unlike in AM CVn-type objects. This difference may be caused by the difficulty of maintaining the hot state.

As a result of our analyses by the PDM method and the $O-C$ diagrams, we could estimate the mean superhump periods. The periods of stage A, B, and C in 2014 are 0.017669(24), 0.017241(18) and 0.017218(5) d, respectively. Moreover, the periods of stage A and B in 2015 are 0.017591(20) and 0.017237(48), respectively. The period derivatives of stage B $P_{\rm dot}$ are $1.01(29)\times10^{-5}$ in 2014 and $1.76(37)\times10^{-5}$ in 2015. Assuming that the stage B continued before the dips, the re-estimated $P_{\rm dot}$ in 2014 is $1.76(12)\times10^{-5}$. This value and $P_{\rm dot}$ in 2015 are consistent with the $P_{\rm dot}$ in 2012 of $2.0(0.2)\times10^{-5}$.

By the new method using the period of stage A superhumps, we obtained the mass ratios of CR Boo, q=0.101(4) in 2014 and 0.087(3) in 2015, respectively. We adopted the former value because of the more clear $O-C$ diagram as described in section 4.2. This mass ratio was confirmed to lie on the theoretical evolutionary path. To verify the theory, more measurements of the mass ratios of AM CVn-type objects are needed. It is expected that this method will be applied to many objects which show superoutbursts regardless of whether the objects are hydrogen-rich or helium-rich.

Acknowledgments

This work was supported by the Grant-in-Aid Initiative for High-Dimensional Data-Driven Science through Deepening of Sparse Modeling (25120007) from the Ministry of Education, Culture, Sports, Science and Technology (MEXT) of Japan. We acknowledge with thanks the variable-star observations by observers worldwide and used in this research.

References

Cleveland, W. S. 1979, J. Amer. Statist. Assoc., 74, 829
Copperwheat, C. M., et al. 2011, MNRAS, 410, 1113
Deloye, C. J., Taam, R. E., Winisdoerffer, C., & Chabrier, G. 2007, MNRAS, 381, 525
Faulkner, J., Flannery, B. P., & Warner, B. 1972, ApJ, 175, L79
Fernie, J. D. 1989, PASP, 101, 225
Green, R. F., Schmidt, M., & Liebert, J. 1986, ApJS, 61, 305
Hirose, M., & Osaki, Y. 1990, PASJ, 42, 135
Honeycutt, R. K., Adams, B. R., Turner, G. W., Robertson, J. W., Ost, E. M., & Maxwell, J. E. 2013, PASP, 125, 126
Kato, T. 2015, PASJ, 67, 108
Kato, T., & Kunjaya, C. 1995, PASJ, 47, 163
Kato, T., & Osaki, Y. 2013, PASJ, 65, 115
Kato, T., Nogami, D., Baba, H., Masuda, S., Matsumoto, K., & Kunjaya, C. 1999, in Disk Instabilities in Close Binary Systems, ed. S. Mineshige, & J. C. Wheeler (Tokyo: Universal Academy Press), p. 45
Kato, T., Stubbings, R., Monard, B., Butterworth, N. D., Bolt, G., & Richards, T. 2004a, PASJ, 56, S89
Kato, T., Uemura, M., Ishioka, R., Nogami, D., Kunjaya, C., Baba, H., & Yamaoka, H. 2004b, PASJ, 56, S1
Kato, T., et al. 2015, PASJ, 67, 105
Kato, T., et al. 2013, PASJ, 65, 23
Kato, T., et al. 2014a, PASJ, 66, 30
Kato, T., et al. 2009, PASJ, 61, S395
Kato, T., et al. 2010, PASJ, 62, 1525
Kato, T., et al. 2014b, PASJ, 66, L7
Levitan, D., Groot, P. J., Prince, T. A., Kulkarni, S. R., Laher, R., Ofek, E. O., Sesar, B., & Surace, J. 2015, MNRAS, 446, 391
Levitan, D., et al. 2011, ApJ, 739, 68
Lubow, S. H. 1991a, ApJ, 381, 259
Lubow, S. H. 1991b, ApJ, 381, 268
Lubow, S. H. 1992, ApJ, 401, 317
Marsh, T. R. 1999, MNRAS, 304, 443
Marsh, T. R., & Horne, K. 1988, MNRAS, 235, 269
Nelemans, G. 2005, in ASP Conf. Ser. 330, The Astrophysics of Cataclysmic Variables and Related Objects, ed. J.-M. Hameury, & J.-P. Lasota (San Francisco: ASP), p. 27
Nelemans, G. 2013, in 9th LISA Symposium, ed. G. Auger, P. Binétruy, & E. Plagnol Vol. 467 of Astronomical Society of the Pacific Conference Series(. p. 27
Nelemans, G., Portegies Zwart, S. F., Verbunt, F., & Yungelson, L. R. 2001, A&A, 368, 939
Nogami, D., Monard, B., Retter, A., Liu, A., Uemura, M., Ishioka, R., Imada, A., & Kato, T. 2004, PASJ, 56, L39
Osaki, Y. 1989, PASJ, 41, 1005
Osaki, Y. 1995, PASJ, 47, L11
Patterson, J. 1999, in Disk Instabilities in Close Binary Systems, ed. S. Mineshige, & J. C. Wheeler (Tokyo: Universal Academy Press), p. 61
Pearson, K. J. 2007, MNRAS, 379, 183
Provencal, J. L., et al. 1997, ApJ, 480, 383
Ramsay, G., Barclay, T., Steeghs, D., Wheatley, P. J., Hakala, P., Kotko, I., & Rosen, S. 2011, MNRAS, 419, 2836
Roelofs, G. H. A., Groot, P. J., Benedict, G. F., McArthur, B. E., Steeghs, D., Morales-Rueda, L., Marsh, T. R., & Nelemans, G. 2007, ApJ, 666, 1174
Roelofs, G. H. A., Groot, P. J., Marsh, T. R., Steeghs, D., Barros, S. C. C., & Nelemans, G. 2005, MNRAS, 361, 487
Roelofs, G. H. A., Groot, P. J., Marsh, T. R., Steeghs, D., & Nelemans, G. 2006a, MNRAS, 365, 1109
Roelofs, G. H. A., Groot, P. J., Nelemans, G., Marsh, T. R., & Steeghs, D. 2006b, MNRAS, 371, 1231
Savonije, G. J., de Kool, M., & van den Heuvel, E. P. J. 1986, A&A, 155, 51
Solheim, J.-E. 2010, PASP, 122, 1133
Solheim, J.-E., & Yungelson, L. R. 2005, in ASP Conf. Ser. 334, 14th European Workshop on White Dwarfs, ed. D. Koester, & S. Moehler

(San Francisco: ASP), p. 387
Stellingwerf, R. F. 1978, ApJ, 224, 953
Sterken, C., 2005, ASPC, 335, 3
Tsugawa, M., & Osaki, Y. 1997, PASJ, 49, 75
Warner, B. 1995, Ap&SS, 225, 249
Warner, B. 2015, Mem. Soc. Astron. Ital., 86, 129
Whitehurst, R. 1988, MNRAS, 232, 35
Wood, M. A., Winget, D. E., Nather, R. E., Hessman, F. V., Liebert, J., Kurtz, D. W., Wesemael, F., & Wegner, G. 1987, ApJ, 313, 757
Zapolsky, H. S., & Salpeter, E. E. 1969, ApJ, 158, 809

Table 1. Log of observations of CR Boo in 2014 April–May.

Start*	End*	mag†	error‡	N§	obs‖	sys#	Start*	End*	mag†	error‡	N§	obs‖	sys#
54.1681	54.2967	1.4740	0.0100	165	OKU	C	64.0963	64.1686	0.7480	0.0090	23	OKU	C
54.1700	54.3069	15.6650	0.0090	283	Ioh	C	64.7275	64.8408	14.9930	0.0220	52	HaC	CV
55.1924	55.2802	2.3700	0.0070	77	OKU	C	64.7892	64.8750	14.7920	0.0030	173	OkC	CV
55.7550	55.8673	17.2140	0.0200	43	HaC	CV	65.3605	65.4357	14.7690	0.0020	195	Kai	C
56.2237	56.3082	2.8860	0.0130	74	OKU	C	65.6687	65.8750	14.4710	0.0020	413	OkC	CV
56.3065	56.3710	6.3280	0.0150	88	CRI	C	66.5911	66.8764	15.0500	0.0080	1000	LCO	CV
56.7574	56.8646	17.2820	0.0190	36	HaC	CV	66.7220	66.8749	15.2100	0.0070	339	HaC	CV
57.0446	57.1938	4.3200	0.0080	359	KU1	C	67.1764	67.1859	0.5660	0.0050	14	OKU	C
57.1928	57.2818	1.9790	0.0070	76	OKU	C	67.3282	67.4310	2.7110	0.0020	121	DPV	C
57.3192	57.3727	5.0500	0.0120	73	CRI	C	67.7191	67.8326	14.8960	0.0050	52	HaC	CV
57.3939	57.6675	15.4880	0.0120	713	Kai	C	68.3276	68.5555	3.0730	0.0030	260	Nov	C
57.7470	57.8625	14.6610	0.0030	52	HaC	CV	68.7163	68.8288	14.6760	0.0050	42	HaC	CV
57.9936	58.2124	14.7350	0.0070	477	Kis	C	69.2196	69.2735	0.4550	0.0050	50	OKU	C
58.0558	58.3436	14.0390	0.0050	656	Mdy	C	69.7137	69.8253	14.8100	0.0030	42	HaC	CV
58.1756	58.2641	-0.2750	0.0030	213	OKU	C	69.7385	69.8607	14.7300	0.0020	248	OkC	CV
58.1996	58.3214	1.9020	0.0030	267	KU1	C	70.1754	70.2336	0.4130	0.0020	54	OKU	C
58.2946	58.3719	3.4020	0.0040	196	CRI	C	70.7109	70.7895	14.7150	0.0030	28	HaC	CV
58.3278	58.6227	2.0000	0.0020	579	Mas	C	70.7760	70.8544	14.6670	0.0020	158	OkC	CV
58.3346	58.5850	3.3090	0.0020	651	CRI	C	71.1723	71.2848	0.3800	0.0020	127	OKU	C
58.3985	58.6691	14.0720	0.0020	1314	Kai	C	72.0138	72.1165	15.2100	0.0030	229	Kis	C
58.7441	58.8598	14.0730	0.0050	55	HaC	CV	72.0258	72.1514	14.6300	0.0010	253	Mdy	C
58.7627	58.8750	14.0780	0.0030	211	OkC	CV	72.8358	72.8542	14.7710	0.0040	38	OkC	CV
59.0349	59.2980	13.9560	0.0020	521	Ioh	C	72.9834	73.0712	15.3350	0.0070	198	Kis	C
59.0736	59.2187	1.9450	0.0020	371	KU1	C	73.1046	73.2750	14.7160	0.0040	324	Ioh	C
59.1364	59.2625	-0.1720	0.0020	297	OKU	C	73.1143	73.2392	0.4660	0.0020	171	OKU	C
59.3580	59.4768	2.1270	0.0020	236	Mas	C	73.1531	73.2165	2.6860	0.0080	142	KU1	C
59.4124	59.5071	14.1520	0.0020	256	Kai	C	73.7512	73.8498	14.8390	0.0020	200	OkC	CV
59.7413	59.8569	14.2090	0.0040	56	HaC	CV	73.9802	74.0260	15.3850	0.0040	103	Kis	C
60.0589	60.2530	14.1050	0.0040	206	Ioh	C	73.9960	74.1623	14.7470	0.0030	321	Ioh	C
60.1337	60.2739	14.7650	0.0050	146	Kis	C	74.0361	74.1370	2.6890	0.0030	260	KU1	C
60.1680	60.2072	-0.0310	0.0070	35	OKU	C	74.1611	74.2474	0.5920	0.0040	79	OKU	C
60.3096	60.4041	2.6880	0.0100	66	Nov	C	74.7513	74.8542	14.8990	0.0020	207	OkC	CV
60.3930	60.8542	14.4370	0.0090	116	HaC	CV	74.9662	75.1626	14.8880	0.0020	380	Ioh	C
60.7138	60.8864	14.2750	0.0020	350	OkC	CV	75.3170	75.4251	2.8840	0.0030	136	DPV	C
62.0043	62.1320	14.9800	0.0030	284	Kis	C	75.7166	75.8543	16.3490	0.0060	274	OkC	CV
62.0579	62.1220	2.3100	0.0040	144	KU1	C	76.7482	76.8539	16.9250	0.0050	125	OkC	CV
62.1143	62.2780	0.1150	0.0030	184	OKU	C	77.4193	77.5626	1.4870	0.0060	146	CRI	C
62.7587	62.8731	14.5580	0.0020	231	OkC	CV	77.7527	77.8545	17.0250	0.0070	97	OkC	CV
63.0037	63.0701	2.5530	0.0110	101	KU1	C	79.3313	79.4719	0.2680	0.0090	172	CRI	C
63.0319	63.1676	15.3350	0.0100	294	Kis	C	80.0446	80.0799	4.8470	0.0220	81	KU1	C

*JD−2456700.

†Mean magnitude.

‡1 σ of the mean magnitude.

§Number of observations.

‖Observer's code: Kis (S. Kiyota), Ioh (H. Itoh), OKU (Osaka Kyoiku U. team), HaC (F. J. Hambsch), CRI (Crimean Astrophys. Obs.), KU1 (Kyoto U. team), Kai (K. Kasai), Mdy (Y. Maeda), Mas (G. Masi), OkC (A. Oksanen), LCO (C. Littlefield), Nov (R. Novak), DPV (P. Dubovsky)

#Filter. "C" means no filter (clear).

Table 2. Log of observations of CR Boo in 2015 May–June.

Start*	End*	mag†	error‡	N§	obs‖	sys#
68.9675	69.2310	3.656	0.009	451	KU1	C
69.3674	69.4176	16.924	0.031	23	COO	CV
69.6436	69.6979	16.727	0.027	44	COO	CV
69.6906	69.8657	16.627	0.009	154	COO	CV
69.9616	70.2212	3.180	0.008	572	KU1	C
70.0089	70.0122	4.316	0.009	10	OKU	C
70.3539	70.5471	16.751	0.009	457	Kai	C
70.4783	70.7267	17.073	0.036	78	HaC	CV
71.3486	71.4785	4.172	0.014	138	DPV	C
71.4765	71.7232	17.398	0.066	64	HaC	CV
71.6371	71.7719	16.944	0.030	87	COO	CV
71.9593	72.2293	3.084	0.019	501	KU1	C
71.9597	71.9630	5.032	0.040	10	OKU	C
72.3420	72.4876	14.857	0.020	143	Kai	C
72.4770	72.7205	14.497	0.011	55	HaC	CV
72.5776	72.7845	0.504	0.003	219	DKS	C
72.7101	72.9055	14.112	0.008	151	COO	CV
73.9596	74.2278	0.754	0.005	387	KU1	C
74.0005	74.0801	13.833	0.007	67	COO	V
74.0044	74.2081	1.837	0.002	544	OKU	C
74.4760	74.7158	14.195	0.004	81	HaC	CV
75.3507	75.4986	0.770	0.003	192	DPV	C
75.6881	75.7365	14.291	0.006	171	COO	CV
76.3280	76.4669	0.903	0.004	168	CRI	C
76.3420	76.4845	0.894	0.003	185	DPV	C
76.4656	76.7113	14.435	0.003	86	HaC	CV
76.4703	76.5224	14.021	0.006	23	COO	CV
76.6661	76.7361	0.221	0.003	52	COO	CV
76.7667	76.8180	14.181	0.004	44	COO	CV
77.0188	77.1308	1.055	0.002	294	KU1	C
80.2850	80.4749	1.276	0.002	241	CRI	C
81.3053	81.4793	1.147	0.006	221	CRI	C
82.3154	82.4890	1.525	0.018	83	CRI	C
83.3337	83.4908	1.231	0.006	138	CRI	C

* JD−2457100.

† Mean magnitude.

‡ 1 σ of the mean magnitude.

§ Number of observations.

‖ Observer's code: L. M. Cook (COO), OKU (Osaka Kyoiku U.), HaC (F. J. Hambsch), CRI (Crimean Astrophys. Obs.), KU1 (Kyoto University), Kai (K. Kasai), DPV (P. Dubovsky), S. Dvorak (DKS)

\# Filter. "C" means no filter (clear).

Table 3. Times of superhump maxima in CR Boo 2014 April–May.

E	maximum time*	error†	$O-C$‡	N§	E	maximum time*	error†	$O-C$‡	N§
0	56758.00770	0.00080	-0.00340	30	236	56762.08140	0.00080	0.00130	62
1	56758.02890	0.00180	0.00060	30	238	56762.11490	0.00040	0.00040	60
4	56758.07860	0.00130	-0.00150	60	240	56762.15170	0.00070	0.00260	18
5	56758.09640	0.00090	-0.00090	64	244	56762.21800	0.00060	-0.00010	19
6	56758.11400	0.00060	-0.00060	62	276	56762.77190	0.00030	0.00220	28
7	56758.13070	0.00100	-0.00110	66	277	56762.78940	0.00030	0.00240	28
8	56758.14890	0.00110	-0.00010	63	278	56762.80620	0.00030	0.00200	27
9	56758.16700	0.00040	0.00070	53	280	56762.84050	0.00030	0.00190	28
10	56758.18560	0.00040	0.00210	88	281	56762.85850	0.00030	0.00260	27
11	56758.20170	0.00040	0.00090	176	445	56765.67670	0.00050	0.01040	19
12	56758.21850	0.00030	0.00050	142	446	56765.69460	0.00030	0.01110	21
13	56758.23610	0.00020	0.00090	99	447	56765.71140	0.00030	0.01070	28
14	56758.25330	0.00020	0.00080	87	448	56765.72850	0.00020	0.01050	28
15	56758.26910	0.00020	-0.00070	66	449	56765.74590	0.00020	0.01060	28
16	56758.28740	0.00020	0.00040	59	450	56765.76350	0.00030	0.01100	28
17	56758.30420	0.00020	0.00000	95	451	56765.78100	0.00020	0.01120	28
18	56758.32080	0.00020	-0.00070	101	452	56765.79800	0.00020	0.01100	28
19	56758.33790	0.00010	-0.00080	101	453	56765.81540	0.00030	0.01120	28
20	56758.35540	0.00010	-0.00050	99	454	56765.83260	0.00020	0.01110	27
21	56758.37250	0.00020	-0.00070	93	455	56765.84970	0.00030	0.01100	28
22	56758.39000	0.00010	-0.00040	64	456	56765.86760	0.00040	0.01170	29
23	56758.40740	0.00020	-0.00030	116	680	56769.74750	0.00030	0.02950	30
24	56758.42490	0.00020	0.00000	135	681	56769.76300	0.00030	0.02780	33
26	56758.45970	0.00010	0.00030	134	682	56769.78220	0.00090	0.02970	32
27	56758.47650	0.00010	-0.00020	133	683	56769.79990	0.00040	0.03010	33
28	56758.49380	0.00010	-0.00010	132	684	56769.81590	0.00030	0.02890	34
29	56758.51090	0.00010	-0.00020	133	685	56769.83260	0.00060	0.02840	31
31	56758.54540	0.00010	-0.00010	132	686	56769.85160	0.00070	0.03020	26
32	56758.56220	0.00030	-0.00070	100	740	56770.78350	0.00050	0.03100	25
33	56758.58000	0.00020	-0.00010	131	741	56770.80080	0.00040	0.03100	29
34	56758.59740	0.00020	0.00010	94	742	56770.81900	0.00060	0.03210	28
35	56758.61460	0.00020	0.00000	94	743	56770.83540	0.00060	0.03120	28
36	56758.63180	0.00020	0.00000	73	744	56770.85280	0.00030	0.03140	25
37	56758.64880	0.00020	-0.00020	66	764	56771.19880	0.00070	0.03250	19
38	56758.66630	0.00040	0.00010	64	765	56771.21570	0.00090	0.03220	19
44	56758.76820	0.00090	-0.00150	15	766	56771.23220	0.00040	0.03150	19
45	56758.78740	0.00040	0.00040	28	817	56772.11370	0.00320	0.03360	55
46	56758.80370	0.00020	-0.00050	35	913	56773.76330	0.00040	0.02810	28
47	56758.82110	0.00020	-0.00040	34	914	56773.78120	0.00060	0.02870	28
48	56758.83830	0.00020	-0.00040	36	915	56773.79770	0.00080	0.02800	27
49	56758.85570	0.00030	-0.00030	36	916	56773.81440	0.00070	0.02740	28
50	56758.87260	0.00020	-0.00060	28	918	56773.84930	0.00050	0.02780	27
60	56759.04470	0.00050	-0.00090	20	971	56774.76160	0.00020	0.02630	24
61	56759.06210	0.00060	-0.00070	26	972	56774.79500	0.00030	0.02530	28
62	56759.07950	0.00030	-0.00060	49	973	56774.81210	0.00040	0.02510	27
63	56759.09670	0.00030	-0.00070	62	975	56774.82980	0.00060	0.02560	28
64	56759.11440	0.00040	-0.00020	64	975	56774.84740	0.00060	0.02590	28
65	56759.13100	0.00030	-0.00080	64	987	56775.05000	0.00060	0.02160	29
67	56759.16500	0.00020	-0.00130	97	988	56775.06920	0.00130	0.02360	29
68	56759.18300	0.00020	-0.00050	98	990	56775.08900	0.00110	0.02610	26
69	56759.19960	0.00020	-0.00120	93	1006	56775.37930	0.00110	0.02330	18
70	56759.21750	0.00020	-0.00050	94	1007	56775.39820	0.00140	0.02500	18
71	56759.23450	0.00020	-0.00080	56	1008	56775.41490	0.00100	0.02450	16
72	56759.25170	0.00020	-0.00080	55	1027	56775.74140	0.00030	0.02340	28
73	56759.26900	0.00020	-0.00070	39	1028	56775.75860	0.00020	0.02340	28
74	56759.28600	0.00030	-0.00100	30	1029	56775.77610	0.00030	0.02360	28
75	56759.30310	0.00040	-0.00110	15	1030	56775.79320	0.00070	0.02340	28
79	56759.37230	0.00030	-0.00090	27	1031	56775.80980	0.00070	0.02280	23
80	56759.38960	0.00020	-0.00090	28	1032	56775.82740	0.00060	0.02320	28
81	56759.40670	0.00020	-0.00100	28	1033	56775.84450	0.00120	0.02310	27
82	56759.42380	0.00020	-0.00110	62	1088	56776.79230	0.00040	0.02250	17
83	56759.44140	0.00020	-0.00070	65	1090	56776.82640	0.00080	0.02210	16
84	56759.45870	0.00020	-0.00070	65	1091	56776.84390	0.00050	0.02250	16
86	56759.49290	0.00030	-0.00090	37	1125	56777.43170	0.00040	0.02400	13
87	56759.51030	0.00040	-0.00080	25	1126	56777.44590	0.00050	0.02100	17
121	56760.09600	0.00060	-0.00140	28	1127	56777.46480	0.00080	0.02260	17
124	56760.14640	0.00080	-0.00260	26	1131	56777.53360	0.00070	0.02240	17
128	56760.21600	0.00050	-0.00200	34	1132	56777.55190	0.00120	0.02360	17
129	56760.23360	0.00050	-0.00170	33	1133	56777.56670	0.00040	0.02100	10
130	56760.25130	0.00040	-0.00120	39	1145	56777.77420	0.00060	0.02170	16
158	56760.73420	0.00020	-0.00110	29	1146	56777.79210	0.00040	0.02230	16
159	56760.75110	0.00020	-0.00140	33	1147	56777.80920	0.00060	0.02220	15
160	56760.76880	0.00020	-0.00100	34	1149	56777.84280	0.00030	0.02130	17
161	56760.78600	0.00020	-0.00100	34	1237	56779.35590	0.00060	0.01720	17
162	56760.80300	0.00030	-0.00130	34	1238	56779.37600	0.00050	0.02000	17
163	56760.82090	0.00040	-0.00060	33	1239	56779.39110	0.00030	0.01790	17
164	56760.83720	0.00040	-0.00150	36	1240	56779.40870	0.00030	0.01830	17
165	56760.85490	0.00040	-0.00110	34	1241	56779.42560	0.00030	0.01790	17
166	56760.87170	0.00030	-0.00140	27	1242	56779.44320	0.00030	0.01830	17
167	56760.88960	0.00030	-0.00080	19	1243	56779.46040	0.00030	0.01820	17

*BJD−2400000.

†Unit: day

‡$C = 2456758.0111 + 0.0172414E$.

§Number of points used to determine the maximum.

Table 4. Times of superhump and orbital hump maxima in CR Boo 2015 May–June.

E	maximum time*	error†	$O-C$‡	N§
0	57168.99429	0.00178	0.02734	36
1	57169.00862	0.00045	0.02442	36
2	57169.02734	0.00049	0.02590	33
8	57169.12903	0.00065	0.02415	33
9	57169.14664	0.00046	0.02451	31
10	57169.16237	0.00056	0.02300	33
42	57169.70687	0.00054	0.01577	16
43	57169.72404	0.00048	0.01570	11
44	57169.74195	0.00047	0.01637	8
45	57169.75781	0.00048	0.01499	13
46	57169.77417	0.00029	0.01411	14
47	57169.79235	0.00108	0.01505	10
48	57169.80858	0.00048	0.01403	11
49	57169.82618	0.00061	0.01439	15
51	57169.86102	0.00043	0.01475	15
63	57170.06509	0.00078	0.01193	36
64	57170.08129	0.00101	0.01089	36
67	57170.13212	0.00037	0.00999	35
156	57171.64934	0.00054	-0.00728	14
185	57172.14455	0.00090	-0.01207	18
214	57172.63720	0.00097	-0.01942	16
220	57172.74279	0.00118	-0.01728	22
223	57172.79327	0.00051	-0.01852	13
290	57173.96716	0.00023	0.00020	28
291	57173.98436	0.00026	0.00016	36
293	57174.01894	0.00017	0.00026	57
294	57174.03623	0.00016	0.00031	47
295	57174.05340	0.00022	0.00023	50
296	57174.07055	0.00023	0.00014	52
297	57174.08743	0.00027	-0.00022	41
298	57174.10491	0.00014	0.00002	43
299	57174.12196	0.00016	-0.00017	73
300	57174.13928	0.00018	-0.00010	62
301	57174.15662	0.00016	-0.00000	72
302	57174.17347	0.00047	-0.00039	70
303	57174.19084	0.00032	-0.00026	43
371	57175.36334	0.00017	-0.00018	18
372	57175.37968	0.00027	-0.00107	18
373	57175.39724	0.00026	-0.00076	18
374	57175.41414	0.00030	-0.00110	17
375	57175.43159	0.00022	-0.00089	18
376	57175.44888	0.00040	-0.00084	18
377	57175.46609	0.00026	-0.00088	18
378	57175.48312	0.00023	-0.00108	18
429	57176.36466	0.00039	0.00115	34
431	57176.39703	0.00040	-0.00097	35
432	57176.41563	0.00032	0.00038	32
433	57176.43177	0.00067	-0.00072	36
434	57176.44981	0.00037	0.00009	35
437	57176.50347	0.00104	0.00202	11
468	57177.03683	0.00030	0.00090	36
469	57177.05359	0.00037	0.00042	37
470	57177.07107	0.00069	0.00066	36
471	57177.08749	0.00055	-0.00017	36
472	57177.10666	0.00029	0.00176	37
473	57177.12330	0.00038	0.00117	37

*BJD−2400000.

†Unit: day

‡$C = 2457168.99251 + 0.0172414E$.

§Number of points used to determine the maximum.